Science Bulletin 64 (2019) 1625–1633

Contents lists available at ScienceDirect

Science Bulletin

journal homepage: www.elsevier.com/locate/scib

Science Bulletin
www.scibull.com

Article

A photothermal reservoir for highly efficient solar steam generation without bulk water

Xuan Wu [a], Ting Gao [a], Chenhui Han [b], Jingsan Xu [b], Gary Owens [a], Haolan Xu [a,*]

[a] Future Industries Institute, University of South Australia, Mawson Lakes Campus, SA 5095, Australia
[b] School of Chemistry, Physics and Mechanical Engineering, Queensland University of Technology, Brisbane, QLD 4001, Australia

ARTICLE INFO

Article history:
Received 8 July 2019
Received in revised form 12 August 2019
Accepted 16 August 2019
Available online 22 August 2019

Keywords:
Solar-steam generation
Photothermal
Aerogel
Solar-thermal energy

ABSTRACT

A solid photothermal reservoir is designed to implement solar-steam generation in the absence of bulk water. The photothermal reservoir is composed of a water absorbing core encapsulated by a photothermal reduced graphene oxide based aerogel sheet which absorbs light and converts it into heat thus evaporating the stored water. The photothermal reservoir is able to store 6.5 times its own weight in water, which is sufficient for one day solar evaporation, thus no external water supplement is required. During solar-steam generation, since no bulk water is involved, the photothermal reservoir minimizes heat conduction loss, and maximizes both of the exposed evaporation surface area and net energy gain from the environment, leading to an energy efficiency beyond the theoretical limit. An extremely high water evaporation rate of 4.0 kg m^{-2} h^{-1} (normalized to projection area) is achieved in laboratory studies over a cylinder photothermal reservoir with a diameter of 5.2 cm and a height of 15 cm under 1.0 sun irradiation. Practical evaluation of the photothermal reservoir outdoors as part of a desalination device demonstrates a similar evaporation rate where the salinity of the clean water produced is lower than 24 ppb. Thus the photothermal reservoir shows great potential for real world applications in portable solar-thermal desalination.

1. Introduction

Solar-steam generation offers an environmentally friendly and cost-effective method of wastewater treatment and clean water production driven by solar energy [1–6]. Over the past a few years, much effort has been devoted to improving the energy efficiency of solar evaporation and facilitating its real-world application. In a solar-steam generation system, photothermal material is the key platform for light-to-heat conversion and steam generation. Various types of photothermal materials including metallic nanostructures [7–15], inorganic semiconductors [16–19], carbon-based nanomaterials [20–39], and polymers [40–44] with broadband light absorption have been investigated to pursue a high evaporation performance. Amongst these well-developed light absorbing materials, carbon-based nanomaterials have become the most prevalent due to their excellent chemical and thermal stability, optical absorption capability, and high light-to-heat conversion efficiency. Another crucial pathway for enhancing the energy efficiency of solar steam generation is optimization of the evaporation configuration/setup. For example, floating photothermal systems instead of conventional dispersion systems were developed to significantly suppress the heat conduction loss to bulk water, thus improving the energy efficiency for solar-steam generation [12,14,15,19,36,42,45]. Thereafter, by introducing the spatially separated evaporation and bulk water surfaces connected by 1D and/or 2D water paths, the heat conduction loss during evaporation process was further decreased [17,25,34,43,46]. Meanwhile, the temperature of evaporation surface can be lowered in such designs, contributing to less radiation and convection losses [18,25,37,47]. Recently, by fully isolating water containing carbon sponges from bulk water, the evaporation rate was increased up to 118% due to the truly heat localized solar evaporation with phased out heat conduction loss [23]. With a smart 3D design of the evaporation surface, the light absorption could be improved due to enhanced light trapping and decreased reflectance loss [18,37]. In these 3D structures, energy gain from the surrounding environment occurs when a temperature deficit exists between the evaporation surfaces without light irradiation and the ambient environment, which significantly improves the evaporation efficiency beyond the theoretical limit.

The achieved progress to date in solar-steam generation provides a fundamental foundation for the design of solar evaporation devices for real-world applications. Currently, the evaporation

* Corresponding author.
E-mail address: haolan.xu@unisa.edu.au (H. Xu).

https://doi.org/10.1016/j.scib.2019.08.022
2095-9273/

device design most commonly advocated requires a rigid container filled with bulk sea/saline water for continuous water supply, a floating photothermal material, and also a chamber to hold the generated clean water. However, in practice, the existence of a bulk saline water significantly increases the risk of re-contaminating the produced clean water and increases the overall weight of the desalination device, which are both important issues for portable solar steam generators. Therefore, a major research goal in promoting the adoption of solar steam generation technologies has been the design of photothermal desalination systems with fewer components and without a bulk saline water reservoir. Such evaporation systems have distinct advantages for energy management because: (1) the heat dissipation by conduction loss is cut off when no bulk water is involved; (2) it is more convenient to design the structure of photothermal materials to optimize the light absorption and energy gain from the surrounding environment for water evaporation. Ideally, developing a single all-in-one component for an in situ photothermal evaporation system which is able to simultaneously serve as a water reservoir, light absorber and steam generator (Fig. 1) would be a major advance in portable steam generator design.

In this work, a solid photothermal reservoir was designed for solar steam generation without the need of bulk water (Fig. 1). The photothermal reservoir was composed of a simple cotton core wrapped in a photothermal aerogel sheet (Fig. 1). The cotton core which has significant water uptake capacity (~6.5 times its own weight) served as a surrogate bulk water reservoir, while the photothermal aerogel sheet assisted in retaining the adsorbed water in the cotton core and simultaneously acted as a light absorber and evaporation surface for the stored water (Fig. 1). The stored water in the photothermal reservoir was sufficient for continuous steam generation under one sun irradiation over one day, and therefore no extra bulk water or additional water supplement was required. This new evaporation design thus exhibited better flexibility for portable solar-steam generation together with an unprecedentedly high energy efficiency for solar-steam generation and clean water production.

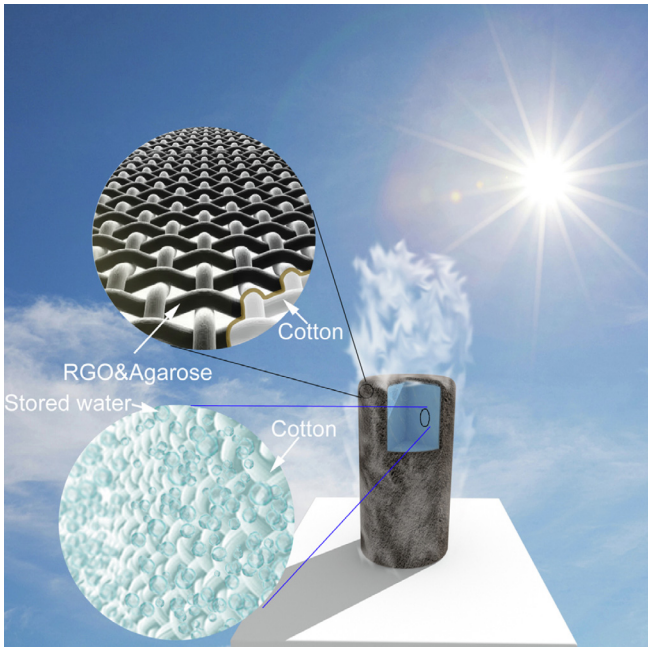

Fig. 1. (Color online) Cartoon illustration of an all-in-one photothermal reservoir for solar steam generation without bulk water. The photothermal reservoir is prepared by encapsulating a cotton core with a photothermal aerogel sheet. The cotton core is able to uptake a large amount of water, while the photothermal sheet contains reduced graphene oxide and agarose assists in retaining the absorbed water and implements the steam generation under sunlight irradiation.

2. Materials and methods

2.1. Materials and chemicals

Commercial cotton sheet and degreased cotton were purchased from local market. Reduced graphene oxide (RGO) was supplied by Huasheng Graphite Co., Ltd., China. Agarose, urea and ethanol were purchased from Sigma-Aldrich. Unless otherwise noted Milli-Q water with a resistance >18.2 MΩ cm^{-1} was used for all experiments.

2.2. Fabrication process

RGO sheets (0.4 g) were dispersed into a 400 mL 7:1 mixture solution of water and ethanol (V_{Water}:$V_{Ethanol}$= 7:1) via ultrasonication. Subsequently, agarose (5 g) and urea (50 g) were added into the solution, which was continuously stirred at 85 °C for 30 min. Thereafter, the resulting hot homogenous suspension was drop-cast onto a piece of cotton sheet (33 × 33 cm). The sample obtained was cooled naturally and frozen at –21 °C in a refrigerator and subsequently freeze dried. The final RGO-agarose-cotton aerogel sheet generated was then washed, tailored and wrapped over the surface of a cotton strand (5 cm in diameter) of varying length (5, 10, 15 cm).

2.3. Characterizations

Scanning electron microscopy (SEM) images were obtained on a Zeiss Merlin scanning electron microscope. Transmission electron microscopy (TEM) images were obtained using a JEOL JEM 2100F transmission electron microscope. X-ray photoelectron spectroscopy (XPS) analysis was carried out on a Kratos Axis Ultra with a Delay Line Detector photoelectron spectrometer using an aluminium monochromatic X-ray source. UV-Vis spectra were recorded using a UV-2600 Spectrophotometer (Shimadzu). Infrared photographs were captured using an IR camera (FLIRE64501). A Dataphysics OCA 20 contact angle system was employed to characterize the hydrophilicity of the samples. Initial concentration of common cations present in seawater (from Semaphore Beach, Adelaide, Australia) were measured using an Inductively Couple Plasma Optical Emission Spectrometry (ICP-OES, Optima 5300V, Perkin Elmer). Following desalination residual ion concentrations in the collected clean water were analyzed using an Inductively Couple Plasma-Mass Spectrometry (ICP-MS) Triple Quad system (ICP-QQQ, Agilent 8800).

2.4. Solar-driven steam generation performance

Solar-driven steam generation was first carried out under laboratory conditions (ambient temperature 25 °C and 30% relative humidity). The photothermal reservoir was initially saturated with a test solution (e.g., fresh water or seawater) and then loaded on to an electronic balance that was connected to a computer to monitor mass loss in real time. A Newport Oriel Solar Simulator (class ABA, 450 W, Newport Oriel 69920) was used as the light source to shine a collimated beam light onto the photothermal reservoir vertically.

Subsequently, seawater evaporation performance was also conducted outdoor in a glass dome (with a hole on the base as clean water outlet) to mimic the real evaporation process over the photothermal reservoir in a natural environment, thereby identifying its practical potential performance for clean water production.

3. Results and discussion

The photothermal aerogel sheet was prepared by a facile drop casting method (Fig. 2a, b). The commercial RGO was used as the photothermal material (Fig. 2c). TEM image reveals that the RGO sample is consisted of free-standing 2D thin sheets with lateral sizes ranging from several hundred nanometers to several micrometers (Fig. 2c). XPS analysis elucidated the reduction degree and chemical state of RGO (Fig. S1 online). XPS peaks at 284.5 and 532.5 eV were attributed to C 1s and O 1s, respectively (Fig. S1a online). The C 1s peaks were evidence of C—C (284.5 eV), C—O (285.7 eV), C=O (286.5 eV) and O—C=O (287.8 eV) functionality in the materials (Fig. S1b online). In comparison to the commonly reported C/O ratio ~2 for GO material [48], element analysis from the survey XPS spectra gave a C/O atomic ratio of 8.84 which demonstrated that the GO was very well reduced. The commercial cotton towel/sheet was used as the flexible substrate. It had a rough hierarchical surface constructed from well-proportioned fabric bundles composed of cotton fibers with width of 8.1–16.5 μm (Figs. 2d and S2 (online)), which resulted in a large surface area, suitable for both enhancing the adhesion of photothermal materials and water evaporation.

By simply casting a hot agarose solution containing RGO onto the cotton sheet followed by self-gelation and freeze drying, a dark black photothermal RGO-agarose-cotton aerogel sheet was prepared (Fig. 2b). It is noticed that coating of cotton sheet with RGO-agarose changed the surface morphology of the fibers of the cotton sheet and a coating layer could be observed (Fig. 2e, f). The inter-fiber space was filled with 2D substance consisting of the RGO and agarose. The surface of the cotton fibers became rough and wrinkled (Fig. 2f), which further increased the surface area, benefiting water evaporation. While the obtained RGO-agarose-cotton aerogel sheet was flexible, lightweight and washable, the RGO was also firmly adhered on the cotton fibers by the agarose. No peeling of black RGO was observed after continued strong finger abrasion over the wetted photothermal sheet (Fig. 2g and Video S1 online). Even after sonicating a piece of RGO-agarose-cotton sheet for 2 cycles (5 min each cycle and the photothermal sheet was kept immersing in water overnight between the two cycles of sonication), no black particles were detached from the photothermal sheet (Fig. S3 online), confirming an excellent mechanical stability. The obtained RGO-agarose-cotton aerogel was hydrophilic due to the hydrophilicity of the constitute cotton and agarose. As shown in Fig. 2h and Video S2 (online), a water droplet was immediately absorbed when it was dropped onto the surface of the photothermal aerogel sheet.

In contrast to the conventional photothermal evaporation surface which is either directly or indirectly in contact with bulk water, in this work, a new evaporation system without bulk water was demonstrated. To realize this, a cotton core made from

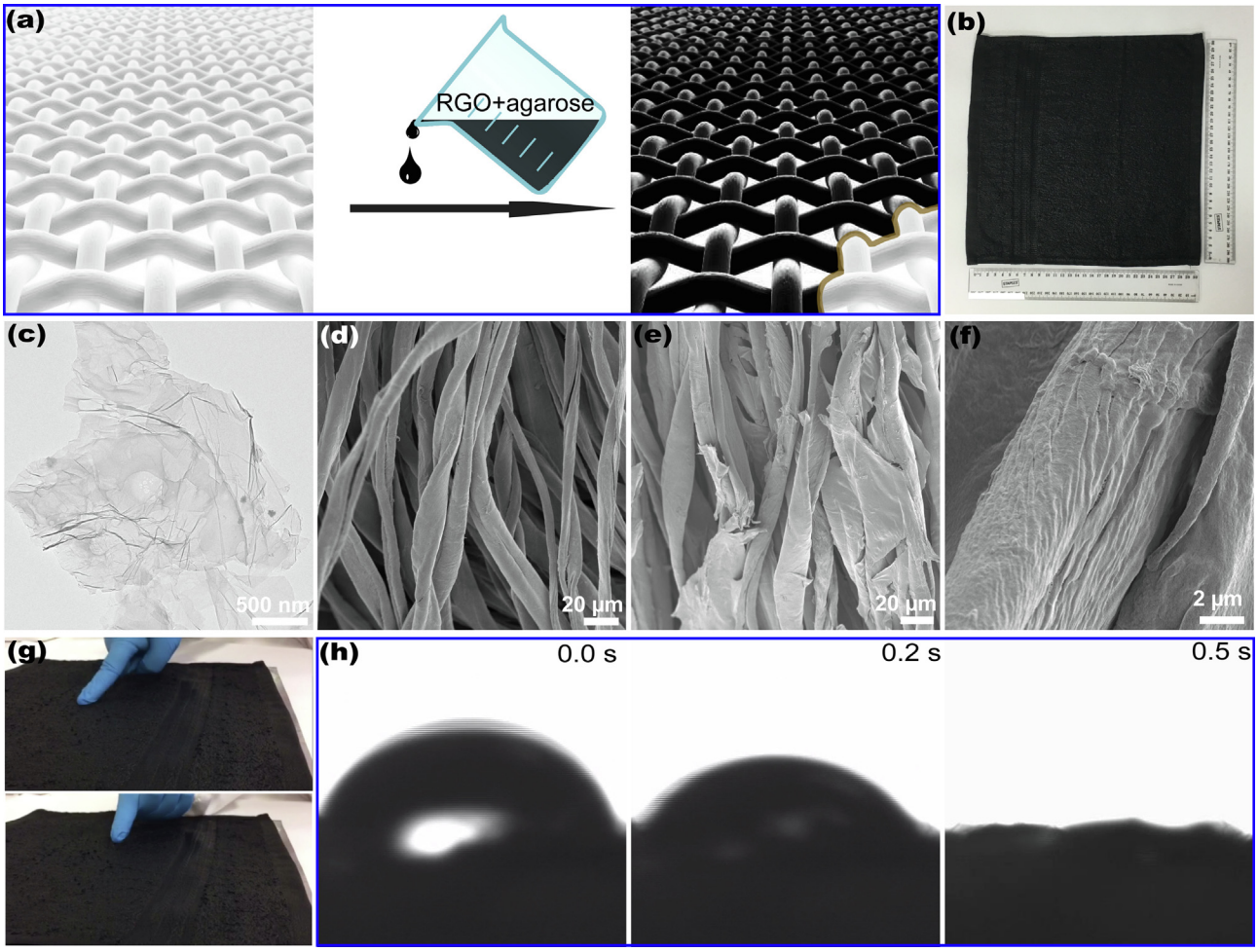

Fig. 2. (Color online) (a) Schematic illustration of the preparation of photothermal RGO-agarose-cotton sheet by a drop casting method; (b) photograph of a obtained photothermal aerogel sheet, (c) TEM image of the commercial RGO sheets. SEM images of the cotton fibers (d) before and (e) after coating of RGO and agarose; (f) high resolution SEM image showing the wrinkled fiber surface after coating of RGO and agarose. (g) Finger abrasion test of the photothermal RGO-agarose-cotton sheet; (h) time-lapse snapshots of absorbing a water droplet by the photothermal aerogel.

commercial degreasing cotton was adopted as a water reservoir (Fig. 3a, b). The cotton core was wrapped in the photothermal RGO-agarose-cotton aerogel sheet to form a single component photothermal reservoir (Fig. 3a, b). Due to the flexibility of the photothermal aerogel sheet, it could be readily cut into the required shapes to fit and wrap the cotton core (Fig. 3b). The prepared cylinder photothermal reservoir could be operated as an all-in-one system, where, with the exception of the bottom surface, light absorption and energy conversion for steam generation was able to take place directly over all of the cylinder surface. This was possible because no part of the cylinder had to be immersed in bulk water. Due to the superhydrophilicity of both the degreasing cotton core and the photothermal aerogel, the photothermal reservoir could easily absorb as much as 6.5 times its own weight in water without visual shape distortion (Fig. 3c, d). For instance, a dried cylinder photothermal reservoir with a diameter of 5.2 cm and a height of 10 cm weighed only 29.70 g (Fig. 3c), making the dried photothermal reservoir light and easy to be carried. However, when it absorbed water to its full capacity, the weight increased to 223.91 g (Fig. 3d), which meant that 194.21 g of water was absorbed and stored ready for solar evaporation. In addition, the photothermal aerogel sheet was able to retain the water securely so that even when the photothermal thermal reservoir was fully absorbed with water, it could be swung and slightly squeezed without any leakage of the stored water (Video S3 online). These merits show excellent benefits for portability and mobility of the device during solar-thermal desalination.

Different from either the 2D flat light absorber floating on water surface or the 3D photothermal cylinders standing in bulk water, the cylinder photothermal reservoir used here requires neither immersion in nor contacting with an external bulk water. The direct result of this is that the available surface for water evaporation and energy absorption both from incident light and environment are greatly enlarged, directly leading to a better evaporation performance. The light absorption ability of the photothermal aerogel sheet was measured across the ultraviolet–visible-near infrared regions (290–1400 nm). As shown in Fig. S4 (online), the photothermal aerogel sheet showed a consistently strong light absorption of >97% across the entire measurement wavelength range, which guarantees the excellent light-to-heat energy conversion.

Solar steam generation over the photothermal reservoir was initially tested under a laboratory condition (Fig. 4a). A Newport Oriel Solar Simulator (class ABA, 450 W, Newport Oriel 69920) with a constant energy output of 1.0 kW m^{-2} was adopted as the light source. The cylinder photothermal reservoir (5.2 cm in diameter and 10 cm in length) was initially saturated with water and placed onto an electronic balance to record mass changes in real-time. An infrared (IR) camera was employed to monitor the surface temperature of the photothermal reservoir during evaporation

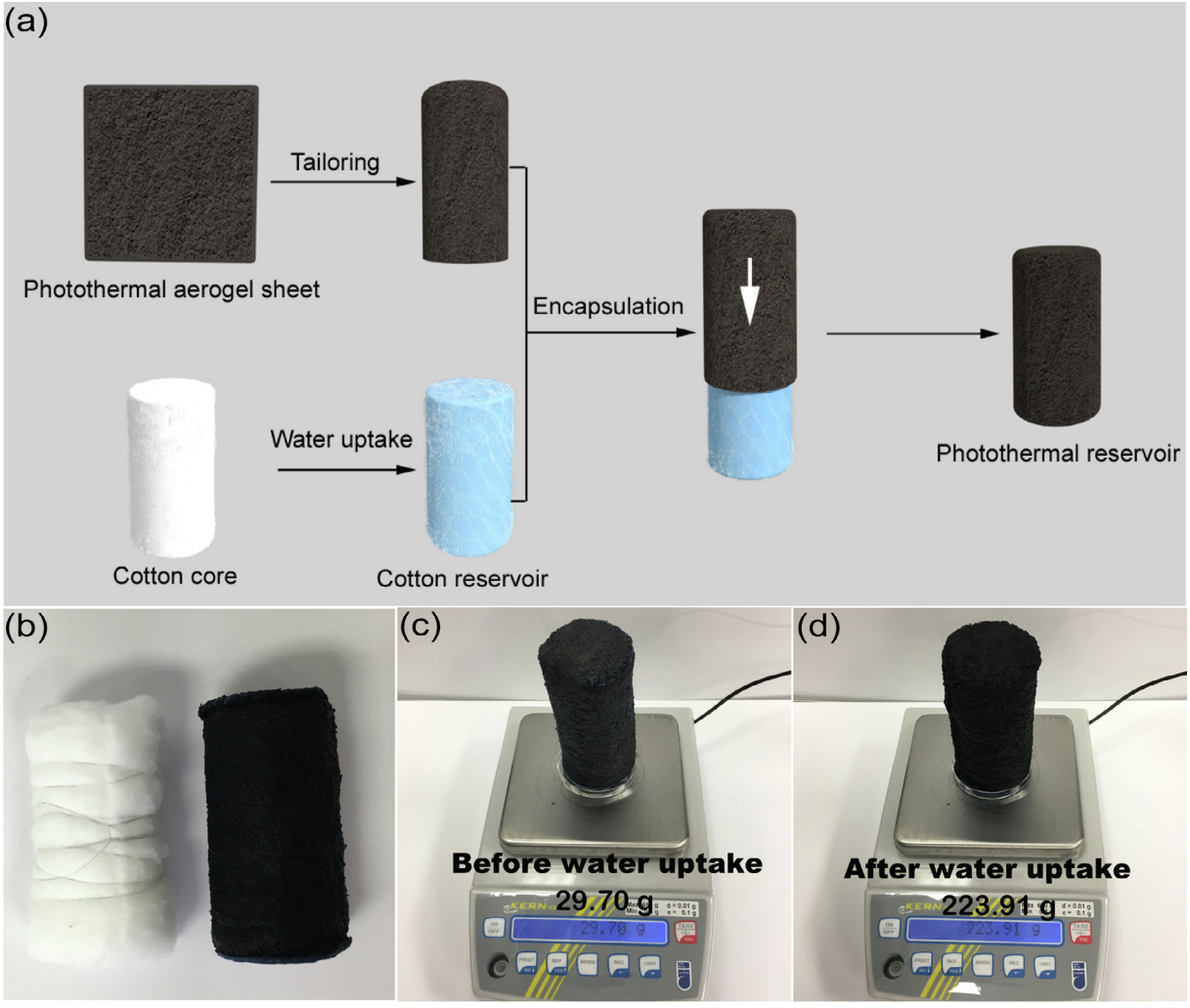

Fig. 3. (Color online) (a) Cartoon illustration of the preparation of a photothermal reservoir; (b) digital photograph of a cotton core and the photothermal aerogel encapsulated cotton core as photothermal reservoir; photograph illustration of the weight change the photothermal reservoir (c) before and (d) after water uptake.

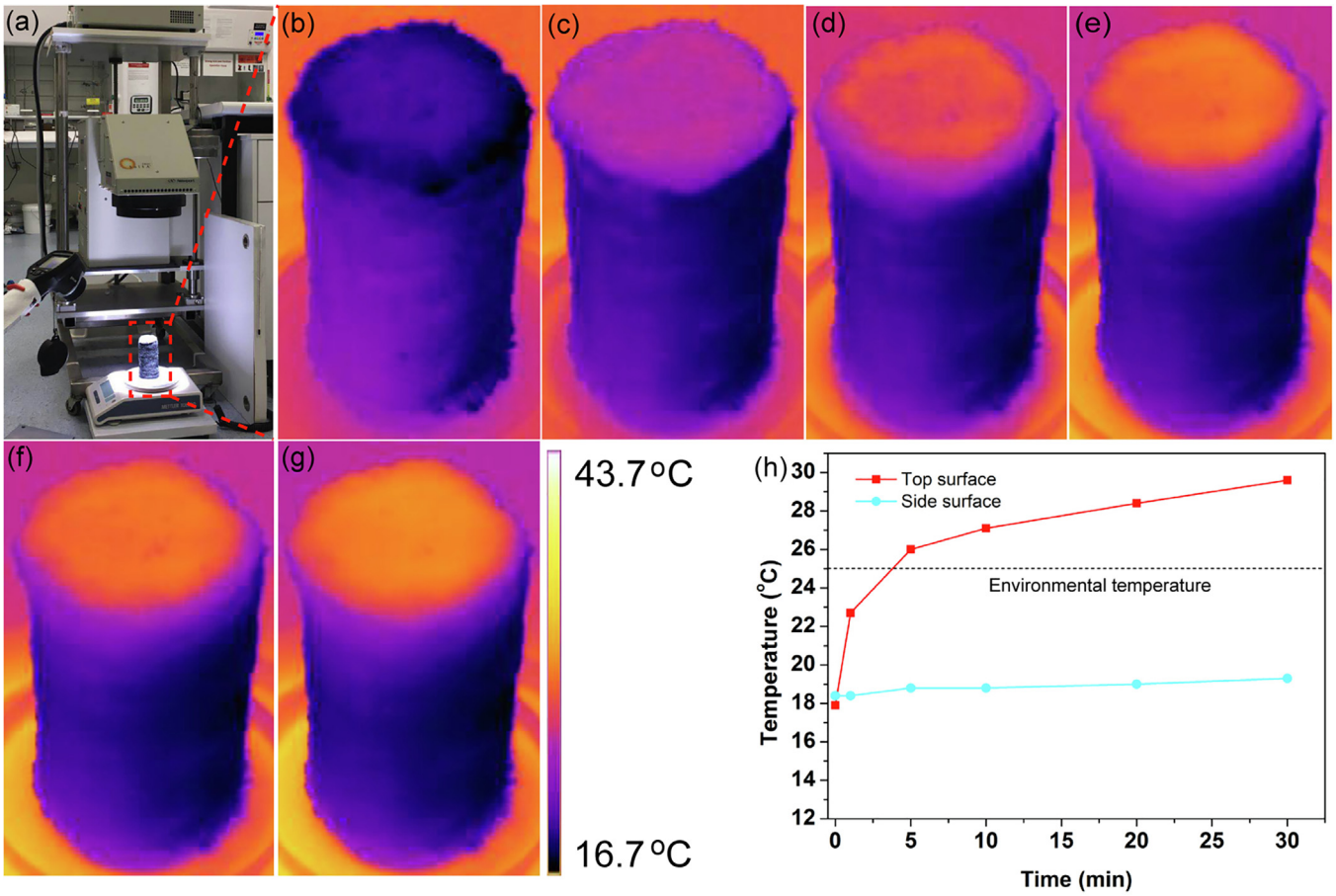

Fig. 4. (Color online) (a) Photography of the solar-steam generation setup; (b–g) IR camera images of the photothermal reservoir during evaporation under 1.0 sun irradiation, the irradiation time is (b) 0 min, (c) 1 min, (d) 5 min, (e) 10 min, (f) 20 min, (g) 30 min, and (h) the corresponding time-dependent average surface temperatures of the top and side surfaces under 1.0 sun irradiation.

process (Fig. 4b–g). Upon light irradiation, the top surface of the cylinder immediately absorbed the incident light and converted it into heat, leading to a rapid increase in surface temperature. As shown in Fig. 4h, the average temperature of the top surface increased to 22.7 °C within 1 min. The average temperature of the top surface became higher than the ambient temperature (25 °C) after 2 min (Fig. 4d, h) and reached a stable temperature of 29.2 °C after 30 min (Fig. 4g, h). Throughout this process, the average surface temperature of the side wall remained at about 19.4 °C (Fig. 4b–h), which was constantly lower than the ambient temperature (25 °C). This temperature deficit resulted in a net energy gain from the surrounding environment [18,37,47], contributing to the overall water evaporation of the cylinder photothermal water reservoir. The applicability of the photothermal reservoir device for practical use was evaluated over a period of 8-hours (1 day) continuous evaporation under 1.0 sun irradiation without additional water supply. The evaporation rate was almost maintained between 3.3 and 3.4 kg m^{-2} h^{-1} (Fig. 5a). This is a very high value compared to those of the 2D and 3D evaporators in the presence of bulk water. About 57 g of water was evaporated over the 8 h period under 1.0 sun irradiation, equivalent to 29.4% of the stored water in the photothermal reservoir. This confirmed that the proposed photothermal reservoir could be safely used for one day solar-steam generation without additional external water supply. During the evaporation, the stored water in the cotton core could be constantly transferred to the photothermal RGO-agarose-cotton aerogel shell to continuously support the evaporation. Fig. 5b depicts the weight loss (i.e., the absorbed water) of the cotton core and photothermal RGO-agarose-cotton aerogel shell separately during the 8 h solar-steam generation, from which one can see that the absorbed water in the cotton core linearly decreased. However the weight of photothermal shell only slightly decreased initially and became stable after 7 h, with a weight (40.97 g) much larger than that of the dried aerogel shell (12.28 g). This confirmed that the water transportation from cotton core to the photothermal aerogel shell was sufficient to support the water evaporation.

Evaporation without light irradiation (dark evaporation) over the same photothermal cylinder was measured to estimate the energy efficiency of the system. A dark evaporation rate of 3.37 g h^{-1} was recorded, thus the net evaporation (with dark evaporation subtracted) over the photothermal reservoir under 1.0 sun irradiation was calculated to be 1.9–2.0 kg m^{-2} h^{-1}.

The solar energy conversion efficiency (η) was estimated using the follow equations:

$$\eta = \frac{m(H_{LV} + Q)}{E_{in}}, \tag{1}$$

$$H_{LV(T)} = 1.91846 \times 10^6 [T_1/(T_1 - 33.91)]^2, \tag{2}$$

$$Q = c(T_1 - T_0), \tag{3}$$

where m is the water evaporation rate (kg m^{-2} h^{-1}) (with the dark evaporation over the sample subtracted), H_{LV} is the latent heat that is required for vaporization of water (J kg^{-1}), T_1 is the temperature

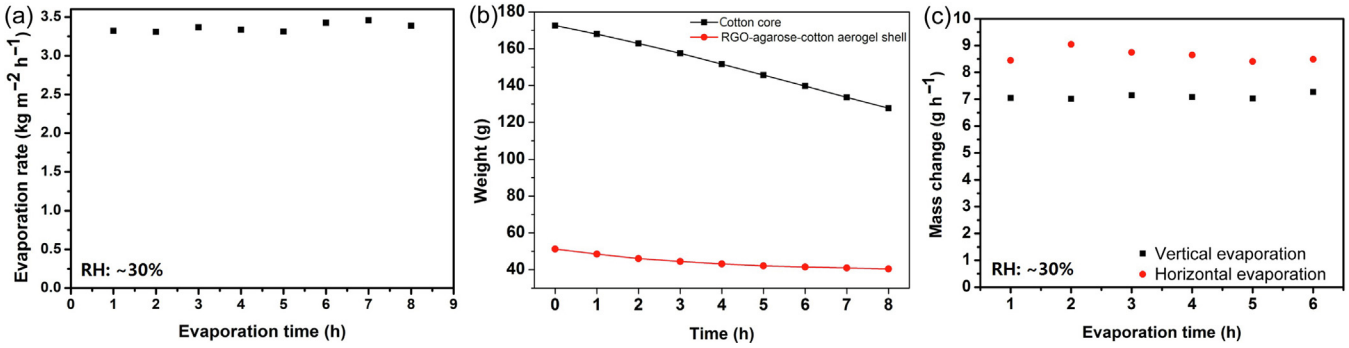

Fig. 5. (Color online) (a) Water evaporation rate of the photothermal reservoir (5.2 cm in diameter and 10 cm in height), (b) mass loss of the cotton core and photothermal RGO-agarose-cotton aerogel shell during the solar-steam generation, and (c) rate of mass loss over the vertically and horizontally placed photothermal reservoirs.

of evaporation (K), and Q is the heat for increasing water temperature (J kg^{-1}), c is the specific heat of water which is 4.2 J g^{-1} K^{-1}, T_0 is the initial temperature of water, and E_{in} (kJ m^{-2} h^{-1}) is the energy input of the incident light. Accordingly, assuming 100% energy efficiency of solar-steam generation, the corresponding evaporation rate should be 1.43 kg m^{-2} h^{-1}. Therefore, the actual evaporation rate of the photothermal reservoir under 1.0 sun is about 133%–139% of the theoretical limit.

To explain the extremely high energy efficiency, energy exchange between the evaporation surface and the environment was investigated. During solar-steam generation, the top evaporation surface had a higher temperature T_1 than that of the environment T_E (Fig. 4), energy loss to the environment by convection and radiation occurred, while the side evaporation surface with a lower temperature ($T_2 < T_E$) could gain energy from the environment. The net energy gain ($E_{environment}$) from the environment can be estimated by the following calculation:

$$E_{environment} = -A_1\varepsilon\sigma\left(T_1^4 - T_E^4\right) - A_2\varepsilon\sigma\left(T_2^4 - T_E^4\right) - A_1h(T_1 - T_E) - A_2h(T_2 - T_E), \quad (4)$$

where A_1 is the area of the top surface of the photothermal reservoir (21.23 cm^2), T_1 is the average surface temperature of the top surface (~29.2 °C), A_2 is the surface area of the side wall of the photothermal reservoir (163.2 cm^2), T_2 is the average surface temperature of the side wall (~19.4 °C), T_E is the ambient temperature (25 °C), ε is emissivity of the absorbing surface (~0.90), σ is the Stefan–Boltzmann constant (5.67×10^{-8} W m^{-2} K^{-4}), and h is convection heat transfer coefficient (assumed to be 10 W m^{-2} K^{-1}). According to the above equation, for our evaporation system, radiation loss from the top evaporation surface was estimated to be 0.049 W, while radiation energy gain of the side evaporation surface from surrounding environment was 0.534 W. Convection loss from the top evaporation surface was estimated to be 0.089 W, and convection energy gain of the side evaporation surface from surrounding environment was estimated to be 0.914 W. Therefore, the net energy gain of the photothermal reservoir from the environment was about 1.31 W, which is on the same order of magnitude as the solar light input E_{in} of 2.06 W, thus significantly enhanced the solar-steam generation of the photothermal reservoir. Heat conduction from top surface to the stored water was investigated. A thermocouple was inserted into the middle of the photothermal reservoir to monitor the temperature change of the absorbed water during evaporation (Fig. S5 online). The initial temperature of the stored water was 25.1 °C (Fig. S5a online). Surprisingly, the temperature did not increase but quickly dropped to 19.9 °C after 1 h evaporation (Fig. S5b–d online). This result indicated that during the solar-steam generation, the evaporation surface extracted energy from the stored water because the temperature of the side surface (19.4 °C) was lower than that of the stored water (25.1 °C). It is reasonable to infer that part of the heat from the top evaporation surface may be transferred to the stored water, but it will eventually be extracted by the side surfaces to drive the cold evaporation which has been proved to be with a higher energy efficiency [37,47].

As there is no extra bulk water involved in the solar-steam generation, the photothermal reservoir can be loaded horizontally rather than vertically (Fig. S6 online), which presented a larger surface for light absorption compared to the vertically standing arrangement, contributing to improved water evaporation. Overall a 21% increase in mass loss (i.e, the amount of evaporated water) was achieved for a horizontal evaporation arrangement (Fig. 5c). This advantage renders flexibility in evaporation setup based on the available space. For instance, when there is enough space, horizontal evaporation arrangement could be selected to target more clean water production. Due to the tailorability of both the photothermal aerogel sheet and the cotton core, the height of the photothermal reservoir can be easily adjusted to tune the stored water and evaporation surface area for desirable output. As show in Fig. S7 (online), photothermal reservoirs with a height of 5, 10 and 15 cm (diameter of 5.2 cm) were prepared for steam generation under one sun irradiation. For the 5 cm tall photothermal reservoir, the dry weight was 13.78 g, and it could absorb and store 87.08 g water (Fig. S8a online). The evaporation rate (2.5–2.6 kg m^{-2} h^{-1}) was lower than both of the 10 and 15 cm tall counterparts due to the smaller side area for evaporation and energy gain from environment (Fig. S9 online). The 15 cm photothermal reservoir with a water storage capacity of 262.14 g (Fig. S8b online) achieved the best evaporation performance with an evaporation rate of 3.9–4.0 kg m^{-2} h^{-1} (Fig. S9 online). It should point out that although after subtracting the dark evaporation, the 15 cm photothermal reservoir has a similar net evaporation rate as the 10 cm one, its absolute evaporation rate of 3.9–4.0 kg m^{-2} h^{-1} is a very high value for practical applications under 1.0 sun irradiation.

To evaluate the efficacy of the photothermal reservoir, the quality of the clean water produced from seawater desalination over the photothermal reservoir was investigated via evaporation of a real seawater from Semaphore Beach (Adelaide, Australia). About 33% of the stored seawater was evaporated during the test which was conducted over 10 h under 1.0 sun irradiation, simulating the typical daily natural sunshine irradiation in the Australia environment. As shown in Fig. 6a, no salt deposition on the evaporation surface was observed after 10 h continuous operation. This was because the salt ions in the photothermal reservoir were not saturated after evaporation. Concurrently, because of the excellent water transportation between the photothermal aerogel sheet and cotton core (Fig. 5b), the salt ions could be quickly transferred from the surface to the water reservoir due to the salt concentration gradient, offsetting the localized salinity increase on the

evaporation surface. This was proved by the increased salinity of the water in the cotton core. It was found that after 10 h evaporation, the salt concentration of the remained water in the cotton core was increased by 43.2%, corresponding to a Na^+ concentration of 15,720 ppm which was far below the saturation level (~36,000 ppm at 20 °C). This confirmed that salt ions diffused from the evaporation surface to the stored water during the solar evaporation, thus no salt crystallization and deposition occurred on the evaporation surfaces. The steam generated during the evaporation process was collected and the salinity was measured by ICP-MS. As shown in Fig. 6b, the concentration of Na^+, Ca^{2+}, K^+ and Mg^{2+} in the collected water were only 23.9, 7.34, 25.3 and 0.5 ppb, which was well below the salinity level of drinkable desalinated water defined by the World Health Organization (WHO) standard (https://www.who.int/water_sanitation_health/publications/dwq-guidelines-4/en/), confirming that this new photothermal reservoir is entirely applicable for practical solar-thermal desalination. After 1 day solar evaporation, the photothermal reservoir can be fully recharged by simply immersing it in seawater for <5 min. The stability of the photothermal reservoir for seawater evaporation was evaluated through cycling performance tests (1 h each cycle) under 1.0 sun irradiation. It is showed that during the 74 cycles of test across 9 days, the evaporation rates were stabled in the range of (2.7–3.4) kg m^{-2} h^{-1} (Fig. 6c). The slight fluctuation in evaporation rate was due to the variation of environmental humidity (24%–44% RH, Fig. 6c). A higher environmental humidity led to a lower evaporation rate (Fig. 6c) [47]. However, at the similar environmental humidity level, the evaporation rates in different testing cycles are almost the same, indicating an excellent stability of the photothermal reservoir.

To further demonstrate the potential practical application of the photothermal reservoir for seawater desalination under natural sunlight, a prototype solar-thermal desalination device was subsequently designed. Since no bulk seawater was needed, no water container and water inlet are required and consequently the desalination device could be drastically simplified requiring only a transparent glass shell, a holder for the photothermal reservoir and a base with a hole in the middle to drain and collect the clean water (Fig. 7a). Using this setup, a 10 cm (Fig. S10 online) and 15 cm (Fig. 7b) photothermal reservoir were tested. The outdoor testing occurred from 10 am to 6 pm. After placing the desalination device under natural sunlight, water vapour was quickly generated and condensed on the glass shell (Fig. 7c). The weather conditions including the sunlight intensity and environmental temperature are shown in Fig. 7d. During the tests, 68.13 and 52.72 g of clean water were generated from the devices containing the photothermal reservoir with height of 15 and 10 cm respectively, corresponding to the average evaporation rate of 4.01 and 3.10 kg m^{-2} h^{-1}. In addition, no salt crystals were observed on the surface of the photothermal reservoir after 1 day outdoor evaporation. These results indicate that the photothermal reservoir has great potential for portable seawater desalination.

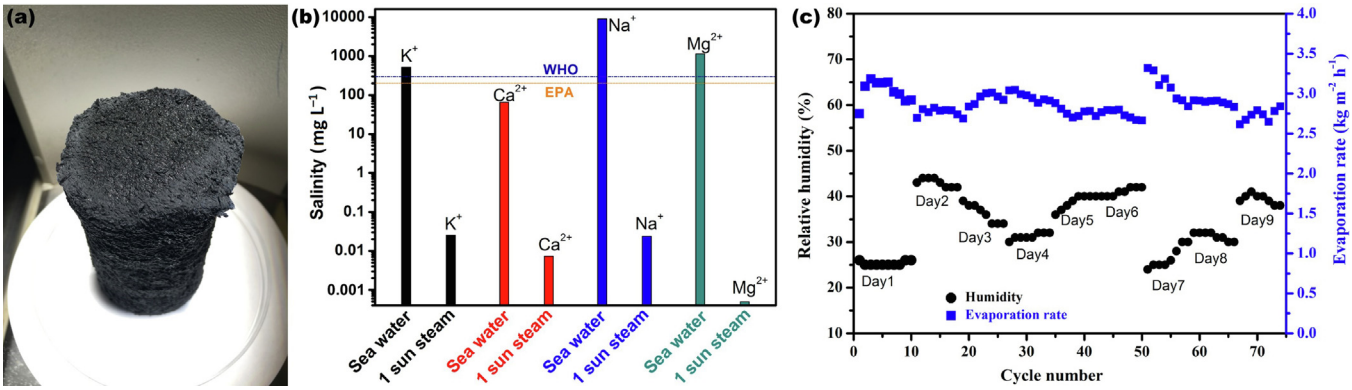

Fig. 6. (Color online) (a) Photograph of the photothermal reservoir after 10 h seawater evaporation. No salt crystals deposition on surface was observed. (b) Main ion concentrations in the original seawater and the collected clean water from solar-steam generation. (c) Evaporation rates over the photothermal reservoir of 74 cycles across 9 days.

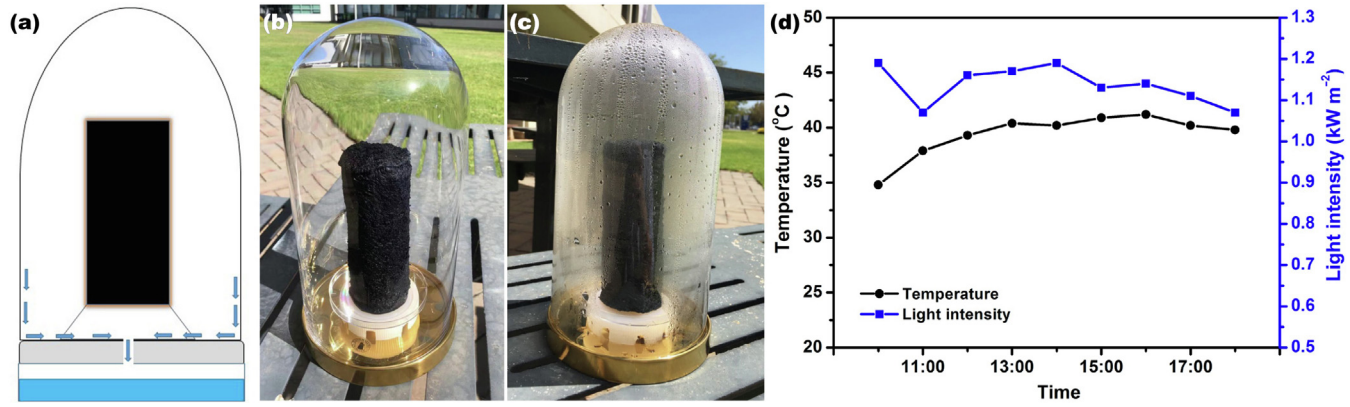

Fig. 7. (Color online) (a) Cross section view of the desalination device; (b) digital photograph of the solar-evaporation device with a photothermal reservoir with a height of 15 cm; (c) photograph showing the clean water condensed on the shell; (d) light intensity and temperature during the outdoor testing.

4. Conclusion

In summary, a photothermal reservoir was successfully developed as an all-in-one evaporator for highly efficient solar-steam generation without bulk water. The photothermal reservoir was composed of a cotton core which is able to absorb and store a large amount of water, encased in a photothermal RGO-agarose-cotton aerogel sheet which served as water retainer, light absorber and evaporation surfaces. An unprecedentedly high solar-steam generation with energy efficiency beyond theoretical limit and a maximum evaporation rate of 4.0 kg m^{-2} h^{-1} over the photothermal reservoir with a height of 15 cm were achieved under 1.0 sun irradiation. The excellent energy efficiency above the theoretical limit was due to the net energy gain from the environment and the stored water through the cool side walls with large surface areas, and the cessation of heat conduction loss. When fully absorbed with water, the photothermal reservoir was sufficient for one day solar-steam generation without additional water supply, leading to a significantly simplified design of the device and the convenience of running the solar-thermal desalination since a bulk seawater container was not required. The photothermal reservoir can be easily recharged by immersing in seawater for a couple of minutes. In addition, there was no risk of the re-containment of the clean water due to spillage of seawater. The Na^+ concentration of the clean water produced from seawater evaporation was only about 23.9 ppb. Thus overall considering these merits, the photothermal reservoir and the proposed device have great potential for practical portable solar-thermal desalination in real world situation.

Conflict of interest

The authors declare that they have no conflict of interest.

Acknowledgments

The authors acknowledge the financial support from University of South Australia, Australia and Huasheng Graphite Co., Ltd., China. We also thank Prof. Shizhang Qiao and Dr. Yao Zhen's help in materials characterization.

Author contributions

Haolan Xu and Xuan Wu conceived and designed the research; Xuan Wu and Ting Gao conducted the experiment; Xuan Wu, Ting Gao, Chenhui Han, Jingsan Xu, Gary Owens and Haolan Xu analyzed and discussed the experimental data; Xuan Wu, Gary Owens and Haolan Xu wrote and revised the paper.

Appendix A. Supplementary data

Supplementary data to this article can be found online at https://doi.org/10.1016/j.scib.2019.08.022.

References

[1] Zhu L, Gao M, Peh CKN, et al. Recent progress in solar-driven interfacial water evaporation: advanced designs and applications. Nano Energy 2019;57:507–18.
[2] Wu X, Chen GY, Owens G, et al. Photothermal materials: a key platform enabling highly efficient water evaporation driven by solar energy. Mater Today Energy 2019;12:277–96.
[3] Wang P. Emerging investigator series: the rise of nano-enabled photothermal materials for water evaporation and clean water production by sunlight. Environ Sci Nano 2018;5:1078–89.
[4] Gao M, Zhu L, Peh CK, et al. Solar absorber material and system designs for photothermal water vaporization towards clean water and energy production. Energy Environ Sci 2019;12:841–64.
[5] Tao P, Ni G, Song C, et al. Solar-driven interfacial evaporation. Nat Energy 2018;3:1031–41.
[6] Zhu L, Gao M, Peh CKN, et al. Solar-driven photothermal nanostructured materials designs and prerequisites for evaporation and catalysis applications. Mater Horiz 2018;5:323–43.
[7] Zhou L, Zhuang S, He C, et al. Self-assembled spectrum selective plasmonic absorbers with tunable bandwidth for solar energy conversion. Nano Energy 2017;32:195–200.
[8] Gao M, Peh CK, Phan HT, et al. Solar absorber gel: localized macro-nano heat channeling for efficient plasmonic au nanoflowers photothermic vaporization and triboelectric generation. Adv Energy Mater 2018;8:1800711.
[9] Zhu M, Li Y, Chen F, et al. Plasmonic wood for high-efficiency solar steam generation. Adv Energy Mater 2018;8:1701028.
[10] Chen C, Zhou L, Yu J, et al. Dual functional asymmetric plasmonic structures for solar water purification and pollution detection. Nano Energy 2018;51:451–6.
[11] Zhou L, Tan Y, Ji D, et al. Self-assembly of highly efficient, broadband plasmonic absorbers for solar steam generation. Sci Adv 2016;2:e1501227.
[12] Zhou L, Tan Y, Wang J, et al. 3D self-assembly of aluminium nanoparticles for plasmon-enhanced solar desalination. Nat Photonics 2016;10:393–8.
[13] Bae K, Kang G, Cho SK, et al. Flexible thin-film black gold membranes with ultrabroadband plasmonic nanofocusing for efficient solar vapour generation. Nat Commun 2015;6:10103.
[14] Ni G, Li G, Boriskina SV, et al. Steam generation under one sun enabled by a floating structure with thermal concentration. Nat Energy 2016;1:16126.
[15] Liu Y, Yu S, Feng R, et al. A bioinspired, reusable, paper-based system for high-performance large-scale evaporation. Adv Mater 2015;27:2768–74.
[16] Zhu L, Sun L, Zhang H, et al. Dual-phase molybdenum nitride nanorambutans for solar steam generation under one sun illumination. Nano Energy 2019;57:842–50.
[17] Wu X, Robson ME, Phelps JL, et al. A flexible photothermal cotton-cus nanocage-agarose aerogel towards portable solar steam generation. Nano Energy 2019;56:708–15.
[18] Shi Y, Li R, Jin Y, et al. A 3D photothermal structure toward improved energy efficiency in solar steam generation. Joule 2018;2:1171–86.
[19] Zeng Y, Yao J, Horri BA, et al. Solar evaporation enhancement using floating light-absorbing magnetic particles. Energy Environ Sci 2011;4:4074–8.
[20] Yang PH, Liu K, Chen Q, et al. Solar-driven simultaneous steam production and electricity generation from salinity. Energy Environ Sci 2017;10:1923–7.
[21] Li J, Du M, Lv G, et al. Interfacial solar steam generation enables fast-responsive, energy-efficient, and low-cost off-grid sterilization. Adv Mater 2018;30:1805159.
[22] Chen Y, Shi Y, Kou H, et al. Self-floating carbonized tissue membrane derived from commercial facial tissue for highly efficient solar steam generation. ACS Sustain Chem Eng 2019;7:2911–5.
[23] Zhu L, Gao M, Peh CKN, et al. Self-contained monolithic carbon sponges for solar-driven interfacial water evaporation distillation and electricity generation. Adv Energy Mater 2018;8:1702149.
[24] Zhao F, Zhou X, Shi Y, et al. Highly efficient solar vapour generation via hierarchically nanostructured gels. Nat Nanotechnol 2018;13:489–95.
[25] Li X, Lin R, Ni G, et al. Three-dimensional artificial transpiration for efficient solar waste-water treatment. Natl Sci Rev 2018;5:70–7.
[26] Zhu MW, Li YJ, Chen G, et al. Tree-inspired design for high-efficiency water extraction. Adv Mater 2017;29:1704107.
[27] Xu N, Hu XZ, Xu WC, et al. Mushrooms as efficient solar steam-generation devices. Adv Mater 2017;29:1606762.
[28] Liu ZJ, Song HM, Ji DX, et al. Extremely cost-effective and efficient solar vapor generation under nonconcentrated illumination using thermally isolated black paper. Global Challenges 2017;1:1600003.
[29] Li YJ, Gao TT, Yang Z, et al. 3D-printed, all-in-one evaporator for high-efficiency solar steam generation under 1 sun illumination. Adv Mater 2017;29:1700981.
[30] Li YJ, Gao TT, Yang Z, et al. Graphene oxide-based evaporator with one-dimensional water transport enabling high-efficiency solar desalination. Nano Energy 2017;41:201–9.
[31] Hu X, Xu W, Zhou L, et al. Tailoring graphene oxide-based aerogels for efficient solar steam generation under one sun. Adv Mater 2017;29:1604031.
[32] Chen CJ, Li YJ, Song JW, et al. Highly flexible and efficient solar steam generation device. Adv Mater 2017;29:1701756.
[33] Wang Y, Zhang L, Wang P. Self-floating carbon nanotube membrane on macroporous silica substrate for highly efficient solar-driven interfacial water evaporation. ACS Sustain Chem Eng 2016;4:1223–30.
[34] Li X, Xu W, Tang M, et al. Graphene oxide-based efficient and scalable solar desalination under one sun with a confined 2D water path. Proc Natl Acad Sci USA 2016;113:13953–8.
[35] Jiang Q, Tian L, Liu KK, et al. Bilayered biofoam for highly efficient solar steam generation. Adv Mater 2016;28:9400–7.
[36] Ghasemi H, Ni G, Marconnet AM, et al. Solar steam generation by heat localization. Nat Commun 2014;5:4449.
[37] Li X, Li J, Lu J, et al. Enhancement of interfacial solar vapor generation by environmental energy. Joule 2018;2:1331–8.
[38] Xu W, Hu X, Zhuang S, et al. Flexible and salt resistant janus absorbers by electrospinning for stable and efficient solar desalination. Adv Energy Mater 2018;8:1702884.
[39] Zhang P, Liu F, Liao Q, et al. A microstructured graphene/poly(n-isopropylacrylamide) membrane for intelligent solar water evaporation. Angew Chem Int Ed 2018;57:16343–7.

[40] Jin Y, Chang J, Shi Y, et al. A highly flexible and washable nonwoven photothermal cloth for efficient and practical solar steam generation. J Mater Chem A 2018;6:7942–9.
[41] Chen QM, Pei ZQ, Xu YS, et al. A durable monolithic polymer foam for efficient solar steam generation. Chem Sci 2018;9:623–8.
[42] Zhang LB, Tang B, Wu JB, et al. Hydrophobic light-to-heat conversion membranes with self-healing ability for interfacial solar heating. Adv Mater 2015;27:4889–94.
[43] Wu X, Wu L, Tan J, et al. Evaporation above a bulk water surface using an oil lamp inspired highly efficient solar-steam generation strategy. J Mater Chem A 2018;6:12267–74.
[44] Wu X, Chen GY, Zhang W, et al. A plant-transpiration-process-inspired strategy for highly efficient solar evaporation. Adv Sustain Syst 2017;1:1700046.
[45] Ito Y, Tanabe Y, Han JH, et al. Multifunctional porous graphene for high-efficiency steam generation by heat localization. Adv Mater 2015;27:4302–7.
[46] Liu P-F, Miao L, Deng Z, et al. A mimetic transpiration system for record high conversion efficiency in solar steam generator under one-sun. Mater Today Energy 2018;8:166–73.
[47] Song H, Liu Y, Liu Z, et al. Cold vapor generation beyond the input solar energy limit. Adv Sci 2018;5:1800222.
[48] Dreyer DR, Park S, Bielawski CW, et al. The chemistry of graphene oxide. Chem Soc Rev 2010;39:228–40.

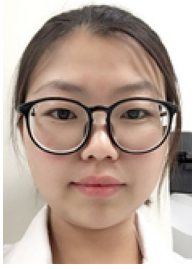

Xuan Wu received her Bachelor degree in Chemistry from Shanxi Normal University in 2010, and Master degree in Physical Chemistry in 2013 from the Tianjin University. She was awarded a Ph.D. degree in Energy and Advanced Manufacturing at the University of South Australia in 2017, and then worked as a Research Associate at the University of South Australia. Her current research interests mainly lie in materials for solar energy conversion and applications.

Haolan Xu is a Senior Research Fellow at Future Industries Institute, the University of South Australia. He obtained his Ph.D. degree at Shanghai Institute of Ceramics, Chinese Academy of Sciences in 2008. Then he worked at Max Planck Institute of Colloids and Interfaces as an Alexander von Humboldt Postdoctoral Fellow. He joined The University of South Australia in January 2011. His research interests include colloid and interface physical chemistry, catalysis, solar-thermal energy conversion and applications.